1

2

3

4

5

6

7

8

9

10

11

12

13

14

15

16

17

18

19

20

High resolution landslide susceptibility mapping using ensemble machine learning and geospatial big data

Nirdesh Sharma[a], Manabendra Saharia[a,b], G.V Ramana[a]

[a]Department of Civil Engineering, Indian Institute of Technology Delhi, Hauz Khas, New Delhi 110016, India

[b]Yardi School of Artificial Intelligence, Indian Institute of Technology Delhi, Hauz Khas, New Delhi 110016, India

Corresponding Author:

Manabendra Saharia

Indian Institute of Technology Delhi

New Delhi, India 110016

Office: +91-011-26591260

Email: msaharia@iitd.ac.in

43 **Abstract**

44 Landslide susceptibility represents the potential of slope failure for given geo-environmental

45 conditions. The existing landslide susceptibility maps suffer from several limitations, such as

46 being based on limited data, heuristic methodologies, low spatial resolution, and small areas of

47 interest. In this study, we overcome all these limitations by developing a probabilistic

48 framework that combines imbalance handling and ensemble machine learning for landslide

49 susceptibility mapping. We employ a combination of One -Sided Selection and Support Vector

50 Machine Synthetic Minority Oversampling Technique (SVMSMOTE) to eliminate class

51 imbalance and develop smaller representative data from big data for model training. A blending

52 ensemble approach using hyperparameter tuned Artificial Neural Networks, Random Forests,

53 and Support Vector Machine, is employed to reduce the uncertainty associated with a single

54 model. The methodology provides the landslide susceptibility probability and a landslide

55 susceptibility class. A thorough evaluation of the framework is performed using receiver

56 operating characteristic curves, confusion matrices, and the derivatives of confusion matrices.

57 This framework is used to develop India's first national-scale machine learning based landslide

58 susceptibility map. The landslide database is carefully curated from global and local

59 inventories, and the landslide conditioning factors are selected from a multitude of geophysical

60 and climatological variables. The Indian Landslide Susceptibility Map (ILSM) is developed at

61 a resolution of $0.001°$ (~100 m) and is classified into five classes: very low, low, medium, high,

62 and very high. We report an accuracy of 95.73%, sensitivity of 97.08%, and matthews

63 correlation coefficient (MCC) of 0.915 on test data, demonstrating the accuracy, robustness,

64 and generalizability of the framework for landslide identification. The model classified 4.75%

65 area in India as very highly susceptible to landslides and detected new landslide susceptible

66 zones in the Eastern Ghats, hitherto unreported in the government landslide records. The ILSM

67 is expected to aid policymaking in disaster risk reduction and developing landslide prediction

68 models.

75 **1   Introduction**

76 Landslides are one of the most devastating geohazards causing acute loss of life and property.

77 According to EM-DAT, landslides are responsible for 17% of natural disaster-related deaths

78 worldwide and billions of dollars in annual damages (CRED, 2022). Recent studies suggest

79 that landslides' frequency and socio-economic impact are increasing with more communities

80 being exposed to landslides (Alimohammadlou et al., 2013; Highland et al., 1998; Yalcin et

81 al., 2011). Moreover, the impact of landslides is often underestimated due to the absence of

82 systematically collected data (Froude and Petley, 2018; Sim et al., 2022). Identification of

83 landslide-prone areas with a high degree of accuracy is necessary to reduce the risk associated

84 with landslides (Azarafza et al., 2021; Castellanos Abella and Van Westen, 2008). With an

85 improvement in computing technology, there is an opportunity to develop an improved

86 landslide susceptibility map by leveraging remote sensing and ground-based datasets as well

87 as state-of-the-art machine learning techniques.

88 Landslides occur when gravity forces pushing on hillslope material exceed the frictional forces

89 holding the material in place, causing slope failure. Landslide susceptibility represents this

90 potential of slope failure (Reichenbach et al., 2018) and a landslide susceptibility map divides

91 the terrain into zones based on the likelihood of landslide occurrence. The landslide

92 susceptibility of any area can be determined before the occurrence of a landslide event by

93 assuming that future landslides would occur under identical conditions as previous landslides

94 (Guzzetti et al., 2006). Landslides are caused by complex interactions of geological,

95 geomorphological, hydrological, and meteorological characteristics. Modeling such complex

96 processes requires sophisticated approaches that can map the non-linear relationships between

97 landslide occurrence and landslide governing variables. To this end, various qualitative and

98 quantitative methods have been developed. The qualitative methods include geomorphological

99 analysis and heuristic methods, whereas the quantitative approaches are based on statistics,

100 physics, or numerical equations (Wieczorek, 1996). The qualitative methods are limited since

101 they are simplistic and based on expert judgement. The quantitative methods can further be

102 classified as physics-based methods and statistical methods. The physics-based methods

103 simulate the physical process to capture the processes leading to slope instability (Li et al.,

104 2016). In contrast, the statistical methods employ data driven approaches to model the landslide

105 process.

106 Machine learning methods are a subset of statistical methods that model the underlying process

107 using data. Machine learning methods are powerful information processing techniques that can

108 augment our understanding of landslide processes. The main advantages of machine learning

109 models include their objectivity, reproducibility, and ability to be continually updated with new

110 data. Once trained, the machine learning models can be used to determine the potential

111 probability of landslides. Earlier studies have compared the utility of various machine learning

112 models in developing landslide susceptibility maps. For instance, Bayesian Network (BN),

113 radial basis function (RBF) classifier, logistic model tree (LMT), and random forest (RF)

114 models (Chen et al., 2018), random forest and XGBoost (Meena et al., 2022), decision tree

115 (DT), support vector machine (SVM), and neuro-fuzzy inference system (ANFIS) (Pradhan,

116 2013), and Support Vector Machines (SVM), Logistic Regression (LR), Fisher's Linear

117 Discriminant Analysis (FLDA), Bayesian Network (BN), and Naïve Bayes (NB) (Pham et al.,

118 2016a) have compared the predictability of machine learning models for landslides prediction.

119 Recently ensembles of multiple machine learning models have been used to develop landslide

120 susceptibility maps, which have achieved an increased accuracy compared to base classifiers

121 (Kavzoglu and Teke, 2022; Sahin, 2020). Although there are many studies which use

122 homogenous landslide susceptibility models and simple ensemble strategies, the heterogenous

123 ensemble learning models are not yet extensively explored for landslide susceptibility mapping

124 (Fang et al., 2021)

125 There have been limited landslide susceptibility studies at high resolution on a national or

126 global scale due to the unavailability of landslide inventories and required computational power

127 (Bălteanu et al., 2010; Okalp and Akgün, 2016). However, with the advent of high-resolution

128 remote sensing and ground mapped geospatial data, it is now possible to develop high

129 resolution landslide susceptibility maps. Currently, most large-scale landslide susceptibility

130 maps are based on heuristic methods and are available at coarse resolution. Some of the large-

131 scale landslide susceptibility maps available in literature are shown in Table 1.

132 **Table 1** Large scale landslide susceptibility maps

Study Area	Resolution	Methodology	Inventory	Reference
Global	1000 m	Heuristic fuzzy	62,898	(Stanley and Kirschbaum, 2017)
Global	1000 m	Weighted linear combination	3000	(Nadim et al., 2006)
Global	0.25°	Weighted linear combination	555	(Hong et al., 2007)
China	0.01°	Artificial Neural Networks	1200	(Liu et al., 2013)
Georgia	100 m	Weighted linear combination	1350	(Gaprindashvili and Van Westen, 2016)
Europe	1000 m	Analytical Hierarchy processes	102000	(Günther et al., 2014)

Iran	85 m	Deep Learning (CNN and RNN)	4069	(Thi Ngo et al., 2021)

To overcome all these shortcomings, we present a general framework consisting of 7 steps: data collection, data preprocessing, machine learning based modelling, hyperparameter tuning, ensemble generation, performance evaluation, output generation and visualization. The framework is deployed for the political boundary of India to generate the India Landslide Susceptibility Map (ILSM), which is India's first national-scale landslide susceptibility map at high resolution (0.001°).

2   Study Area

The study area covers the political boundary of India. India accounts for nearly 8% of global landslide fatalities (Ram and Gupta, 2022). From 2001 through 2021, India's average annual landslide death count is 847, and the average annual financial losses amount to $0.3 billion (CRED, 2022). In 2018 heavy rainfall and landslides caused about 500 casualties in Kerala, Karnataka, and Tamil Nadu (Martha et al., 2021). Recently floods and landslides in Assam killed at least 14 people and displaced 1.7 million people across 29 districts (https://reliefweb.int/disaster/fl-2022-000213-ind).

 India exhibits some of the highest diversity in geology and topography. Due to steep slopes and heavy rainfall most of the landslides occur in the northwest himalayas followed by the northeast himalayas and the western ghats (Martha et al., 2021).

The Himalayas are composed of sedimentary rocks which are prone to denudation and erosion. Furthermore, the steep slopes and rapid flowing rivers cause a large amount of toe erosion making the slope unstable. Therefore, most of the landslides in himalayas are rockfalls. On the contrary western ghats have basalt rocks, and rivers with gentle slopes thereby resulting in fewer rockfalls. However, weathering due to heavy rainfall has led to a development of thick

156 layer of regolith, thereby leading to mudslides (Martha et al., 2021). Another important

157 geological factor is the slope of the terrain. While most of the landslides in the western ghats

158 are associated with steep slopes, most of the landslides in northeast himalayas are associated

159 with gentler slopes due to a compressed fold and fault sequence which leads to reduced shear

160 strength (Martha et al., 2021).

161 Apart from geology, environmental and anthropogenic factors play an important role in the

162 spatio-temporal variability of landslides. Rainfall intensity and duration are the most important

163 environmental factor for triggering landslides, consequently most of the landslides occur on

164 the areas towards the windward side of western ghats and Himalayas. However, the western

165 ghats require less rainfall to trigger landslides when compared to Himalayas due to high soil

166 depth which allows more water retention and an increased porewater pressure ultimately

167 leading to landslides, whereas the Himalayas have exposed rocks which require large rainfall

168 to increase porewater pressure (Martha et al., 2021). Among the anthropogenic factors, road

169 development, construction add to slope instability and increase the risk of landslides e.g. In

170 Sikkim most of the landslides occurred in urban areas which have been attributed to

171 urbanization and infrastructure development (Singh et al., 2020). A more comprehensive

172 review of the spatio-temporal variability of geology and landslides can be found in (Martha et

173 al., 2021; Valdiya, 2015)

174 The landslide maps prepared in India till 2013 are limited to important transportation corridors

175 and discrete locations which witnessed heavy damage due to landslides. In 2013 floods and

176 landslides in Uttarakhand impacted 12 of the 13 districts, caused thousands of deaths, and left

177 nearly 75000 pilgrims stranded (https://reliefweb.int/report/india/uttarakhand-flash-floods-

178 %E2%80%93-report). In response to the Uttarakhand disaster, the Geological Survey of India

179 (GSI) launched the National Landslide Susceptibility Mapping (NLSM) project, which has

180 since produced a 1:50,000 scale landslide susceptibility map of 85% of the total target area in

181   landslide-prone areas ("Lok Sabha," 2021). The NLSM project models susceptibility using an

182   analytic hierarchy process (AHP) where an assigned weight is allocated for various factors

183   based on the Bureau of Indian Standards, (1998) guidelines. The AHP makes the landslide

184   maps subjective and reduces the usability of the model; also since the maps are on a scale of

185   1:50000, smaller landslides cannot be detected ("NDMA," 2019). Therefore, we need a

186   strategy to generate a finer scale susceptibility map for India using data-based methods.

187   **3   Datasets**

188   A wide variety of factors are significant in influencing landslide susceptibility and have been

189   extensively studied (Guzzetti et al., 2006). In landslide susceptibility studies, these parameters

190   are required to model the shear strength of soil, soil-water interaction, soil vegetation

191   interaction, and the impact of anthropogenic activities. The landslide conditioning factors are

192   available in different formats and spatial resolutions.

193   Chang et al. (2019) suggests that susceptibility maps with high resolution topographic data may

194   be inaccurate due to noise in the data, meanwhile when mapping landslide susceptibility at

195   coarse resolution, the number of landslide conditioning factors required is more (Gaidzik and

196   Ramírez-Herrera, 2021). Based on the study area, available spatial resolution, and data

197   availability, we selected 16 landslide conditioning factors at a spatial resolution of 0.001°. The

198   datasets developed are discussed below:

199   **3.1   Landslide Inventory**

200   Landslide inventory is a systematic record of landside location, extent of landslide and other

201   characteristics. Landslide inventory is important for mapping landslide susceptibility, landslide

202   risk, landslide early warning and understanding the evolution of landscapes especially in hilly

203   regions which are dominated by landslides. Developing a Landslide susceptibility is landslide

204 inventory is the primary step towards developing landslide susceptibility since susceptibility is

205 based on the idea that future landslides will occur in similar conditions as past landslides.

206 Landslides cause a discernable impact on the terrain which is used to delineate the geographical

207 extent of these landslides. This extent is then mapped using field surveys, aerial

208 photogrammetry, or satellite imagery. The selection of the mapping technique is based on a

209 multitude of factors such as the size of the study area, data availability, and the availability of

210 resources.

211 In this study, landslide inventory was formed by merging landslide inventories acquired from

212 the Geological Survey of India and the Cooperative Open Online Landslide Repository

213 (COOLR) (Juang et al., 2019). Prior to the widespread availability of high-resolution satellite

214 imagery, the Geological Survey of India (GSI) primarily relied on field surveys to construct

215 landslide inventories. However, this approach posed significant limitations, particularly in

216 regions characterized by mountainous slopes. Following a thorough review of multiple GSI

217 reports, it is evident that contemporary landslide inventories are now predominantly created

218 through multitemporal analysis using Google Earth imagery.

219 Before the advent of high resolution satellite imagery GSI primarily relied on field surveys to

220 construct landslide inventories. However, this approach was costly and posed severe

221 limitations, particularly in inaccessible mountainous regions. Our analysis of multiple

222 landslide reports from GSI leads us to the conclusion that current landslide inventories are

223 developed using multitemporal analysis on Google Earth imagery. Furthermore, to enhance

224 the accuracy of these inventories, some of the accessible landslides are verified through on-

225 site field visits.

226 (https://www.gsi.gov.in/webcenter/portal/OCBIS/pageQuickLinks/pageLandslideHazardRep

227 ort).

228   GSI's landslide inventory contains 49105 landslides mapped as points and 105,224

229   landslides mapped as polygons. COOLR repository, on the other hand, is a citizen science-

230   based landslide repository. The COOLR data selection and preparation are carried out by

231   eliminating data entries whose location is not accurate (Stanley and Kirschbaum, 2017).

232   Figure 1 shows the case study area boundary and the landslide inventory.
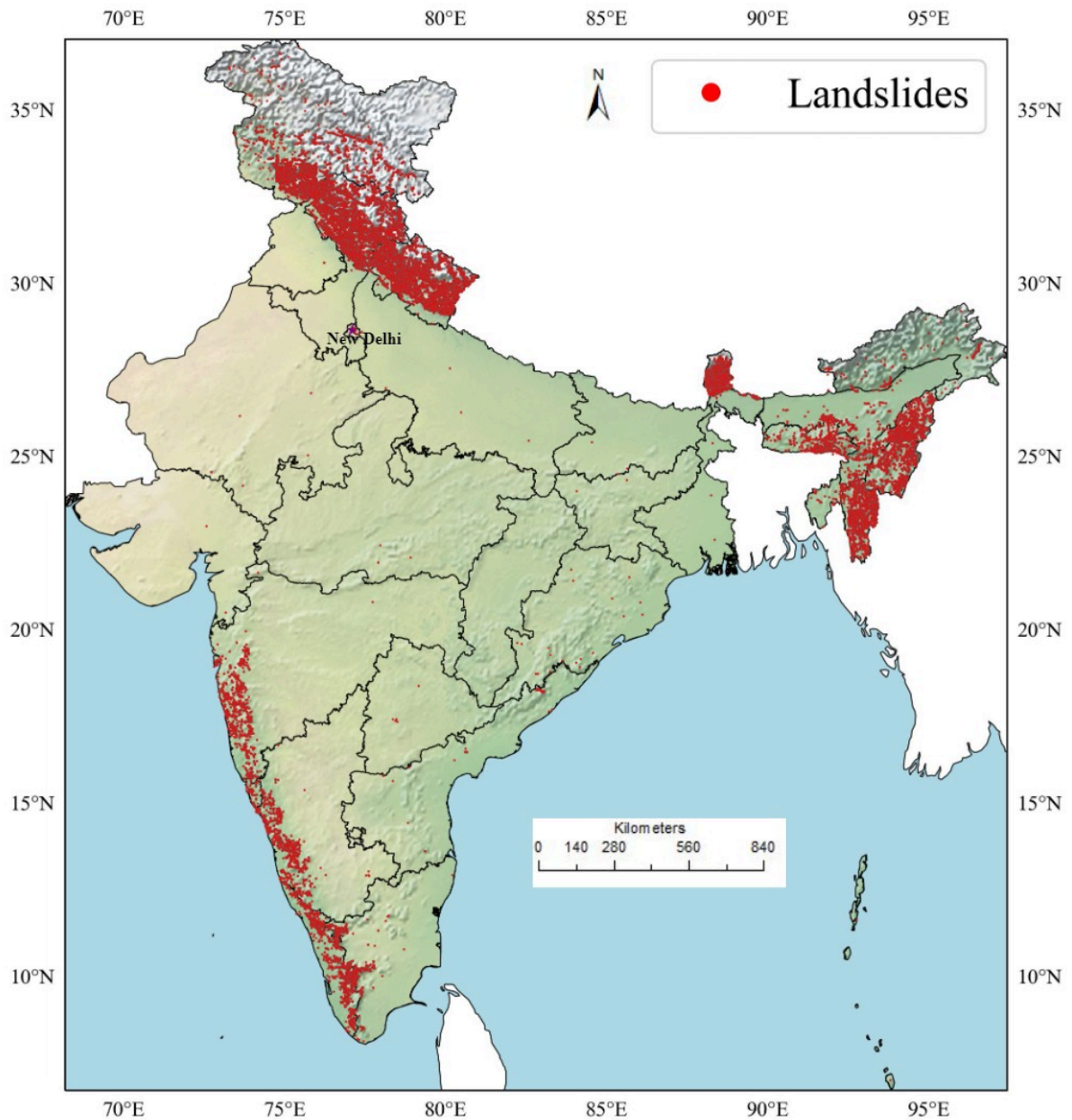
233

234   Figure 1 Landslide inventory for India

3.2 Landslide conditioning factors

A landslide susceptibility model aims to develop a relationship between landslide inventory and landslide conditioning factors. Based on extensive literature review our initial experiments consisted of 19 landslide conditioning factors. Three variables, namely LULC data, distance from faults and drainage density of rivers had zero random forest feature importance. The feature importance was also validated using the global feature importance method Partial Dependence Plots for SVM and ANN. Therefore, we removed these features from landslide conditioning factors database. Finally, we develop 16 landslide conditioning which are shown in Table 2.

Table 2 Landslide Conditioning Factors

Attribute Name	Description	Data Type	Data Source
Elevation	Height in meters	Raster	MERIT DEM (Digital Elevation Model) (Yamazaki et al., 2017)
Slope	Rate of change of elevation	Raster	
Aspect	Direction of slope in degrees	Raster	
TWI	Location of water accumulation	Raster	
Curvature	Shape of slope	Raster	
Upslope Curvature	Average curvature of upslope pixels	Raster	
Downslope Curvature	Average curvature of downslope pixels	Raster	
Sand	Fraction of Sand in the soil	Raster	ISRIC (Laura and de Sousa, 2020; Poggio and de Sousa, 2020a, 2020b)
Silt	Fraction of Silt in the soil	Raster	
Clay	Fraction of clay in the soil	Raster	
Roads	Distance from urban and rural roads	Vector (line)	PMGSY
Rivers	Minor and Major rivers of India	Vector (line)	CWC (Central Water Commission)

Precipitation	Precipitation of the wettest month	Raster	World Clim (Fick and Hijmans, 2017)
NDVI	Area of green vegetation	Raster	MODIS
Landslide Lineament	Zone of faults and Fractures	Vector (line)	GSI
Erosivity factor	India Rainfall Erosivity Dataset	Raster	IIT Delhi (Raj et al., 2022)
Landslide inventory	Database of historical landslides	Vector (Points, Polygons)	GSI

245

246   3.2.1   DEM (Digital Elevation Model)

247 Digital Elevation Models represent the terrain of an area, in the form of a raster grid. DEMs

248 help to identify intricate terrain features for landslide hazards. The input DEM is extracted from

249 MERIT DEM, a high accuracy global DEM at three arc-second resolution developed using

250 multisensor data fusion (Yamazaki et al., 2017). MERIT is designed to improve upon the

251 original SRTM DEM by using advanced techniques to reduce errors and fill gaps in the data.

252 MERIT DEM is significantly improved over flat regions, along with a better representation of

253 rivers and valleys, which is essential for landslide mapping (Yamazaki et al., 2017). DEMs are

254 also used to derive secondary inputs like slope, aspect, curvature, and topographic wetness

255 index. The slope dictates the shear stress and hydrological process, whereas the curvature

256 dictates the weathering and erosion processes. The aspect shows the slope direction and is an

257 essential and complex variable for landslide susceptibility. Aspect is also closely related to

258 climatic conditions especially the variations in solar radiation, soil moisture, and temperature

259 distribution which impact the occurrence of landslides (Cellek, 2021). Since $0°$ aspect and $360°$

260 aspect are identical, the numerical values of the aspect do not accurately depict the aspect value.

261 The aspect was divided into nine directional groups to account for the impact of the aspect

262 (Youssef and Pourghasemi, 2021).

263   The topographical wetness index (TWI) estimates locations where water will accumulate.

264   Consequently, an area with higher TWI will be associated with more landslides. We also

265   include upslope and downslope curvature of pixels to model landslide susceptibility. The

266   average of all hydrologically upslope pixels is represented by upslope curvature, whereas the

267   average of all downslope pixels is represented by downslope curvature. The datasets for slope,

268   aspect, curvature, and Topographic Wetness Index are derived from MERIT DEM in Google

269   Earth Engine (Gorelick et al., 2017).

270   3.2.2   NDVI

271   The Normalized Difference Vegetation Index or NDVI is developed using near-infrared and

272   infrared imagery reflectance since green vegetation strongly absorbs red light and reflects

273   infrared rays. NDVI is an indicator of healthy vegetation and is used to incorporate the

274   vegetation-soil interaction, which is a crucial factor influencing landslides. To develop NDVI

275   map we first calculate the median NDVI for monsoon months from sentinel 2 data after cloud

276   masking. Afterwards we use month wise median of images to get monthly NDVI. This process

277   is repeated for years 2015-2020. The final NDVI map is an average of all the NDVIs.

278   3.2.3   Soil Composition

279   The soil composition, which determines the soil's shear strength and drainage capacity, is an

280   essential factor influencing landslide susceptibility. Fine-grained soils have smaller particle

281   sizes and a higher surface area, making them more prone to erosion and slope failure. They

282   also tend to have lower permeability, meaning they can absorb and drain less water. As a result,

283   they can become saturated with water and lose their stability, leading to landslides.

284   On the other hand, coarse-grained soils have larger particle sizes and a lower surface area,

285   making them more resistant to erosion and slope failure. They also tend to have higher

286   permeability, implying they can absorb and drain water better, which helps stabilize the soil

287   and reduce the risk of landslides.

14

288   Soil properties, namely sand fraction, silt fraction, and clay fraction, are incorporated from the

289   International Soil Reference and Information Centre (ISRIC) soil grids dataset. ISRIC develops

290   soil properties and classes using global covariates and globally fitted models (Laura and de

291   Sousa, 2020; Poggio and de Sousa, 2020b, 2020a).

292   3.2.4   Anthropogenic Factors

293   Anthropogenic interventions such as construction and toe cutting destabilize the slopes leading

294   to landslides. In hilly regions, most landslides occur along transportation corridors since

295   transportation corridors are developed by cutting hills, destabilizing the slope, and thereby

296   causing an increase in the number of landslides. In this study, we use road maps from the

297   GeoSadak platform (https://geosadak-pmgsy.nic.in/), which have been meticulously ground

298   mapped under the directive of the Government of India and contain 1,027,269 major and minor

299   roads mapped as polylines. This data explicitly records rural habitations in distant areas not

300   adequately covered by previous datasets. The road polyline is used to prepare a raster

301   containing the euclidean distance from the nearest road, and this is the first time this detailed

302   road network data has been used for landslide susceptibility studies.

303   3.2.5   Meteorological factors

304   Most slope failures in India are triggered by meteorological events, specifically intense and

305   prolonged rainfall. Heavy precipitation increases soil weight and reduces shear resistance,

306   making the slope vulnerable to failure. To incorporate the impact of precipitation on slope

307   failure, the precipitation of the wettest month from worldclim data is used (Fick and Hijmans,

308   2017; Hijmans et al., 2005). The precipitation of the wettest month from worldclim has been

309   previously utilized in multiple landslide susceptibility studies to account for the spatial

310   distribution of rainfall (Dinanta et al., 2020; Ramachandra et al., 2013).

311   3.2.6   Distance from Rivers

312   Moving water continuously causes soil erosion, removal of toe support, and water seepage

313   from rivers thereby reducing the soil strength and increasing the likelihood of landslides along

314   riverbanks. The euclidean distance to river map is developed using a line map for India's major

315   rivers, minor rivers, and rivulets acquired from the Central Water Commission. The line map

316   is processed to create a raster map of $0.001°$(100 m) resolution where every pixel denotes the

317   euclidean distance from the nearest river.

318   3.2.7   Rainfall erosivity

319   Rainfall erosivity represents the kinetic energy of rainfall intensity. Falling raindrops exert

320   pressure on the surface and cause instability of the soil surface, leading to soil erosion and

321   landslides. Higher rainfall erosivity increases the chance of landslides (Ahmad et al., 2019).

322   Despite its importance, erosivity is a highly underutilized variable in landslide research. In this

323   study, we utilize the Indian Rainfall Erosivity Dataset (IRED), the first national-scale mapping

324   of rainfall erosivity factor (R factor) over India, to incorporate the impact of erosivity on

325   landslides (Raj et al., 2022).

326   3.2.8   Landslide Lineament

327   The structural geology of an area considerably impacts the occurrence of landslides (Anbalagan

328   and Singh, 1996; Ramli et al., 2010). To incorporate the impact of structural geology, we use

329   landslide lineaments which are features caused by joints and faults. The landslide lineament

330   data has been developed by GSI and is available at bhukosh (https://bhukosh.gsi.gov.in/),

331   India's national geological data portal.

332   **4   Methodology**

333   The landslide inventory consists of 105,224 landslides mapped as polygons and 49,105

334   landslides mapped as points from GSI. The COOLR database contains 1820 landslide points,

335   but only 489 landslides are selected for model development since other data points are not

336 mapped accurately enough for high-resolution landslide mapping. The landslide conditioning

337 factors and landslide inventory is divided into pixels of $0.001°*0.001°$. If any pixel has a point

338 landslide, landslide conditioning factors of the pixel are assumed to be landslide causing. In

339 case of polygon data, all the pixels covered by landslide polygon were assumed to be landslide

340 pixels. The overall methodology followed to develop a high-resolution landslide susceptibility

341 map is shown in Figure 2.
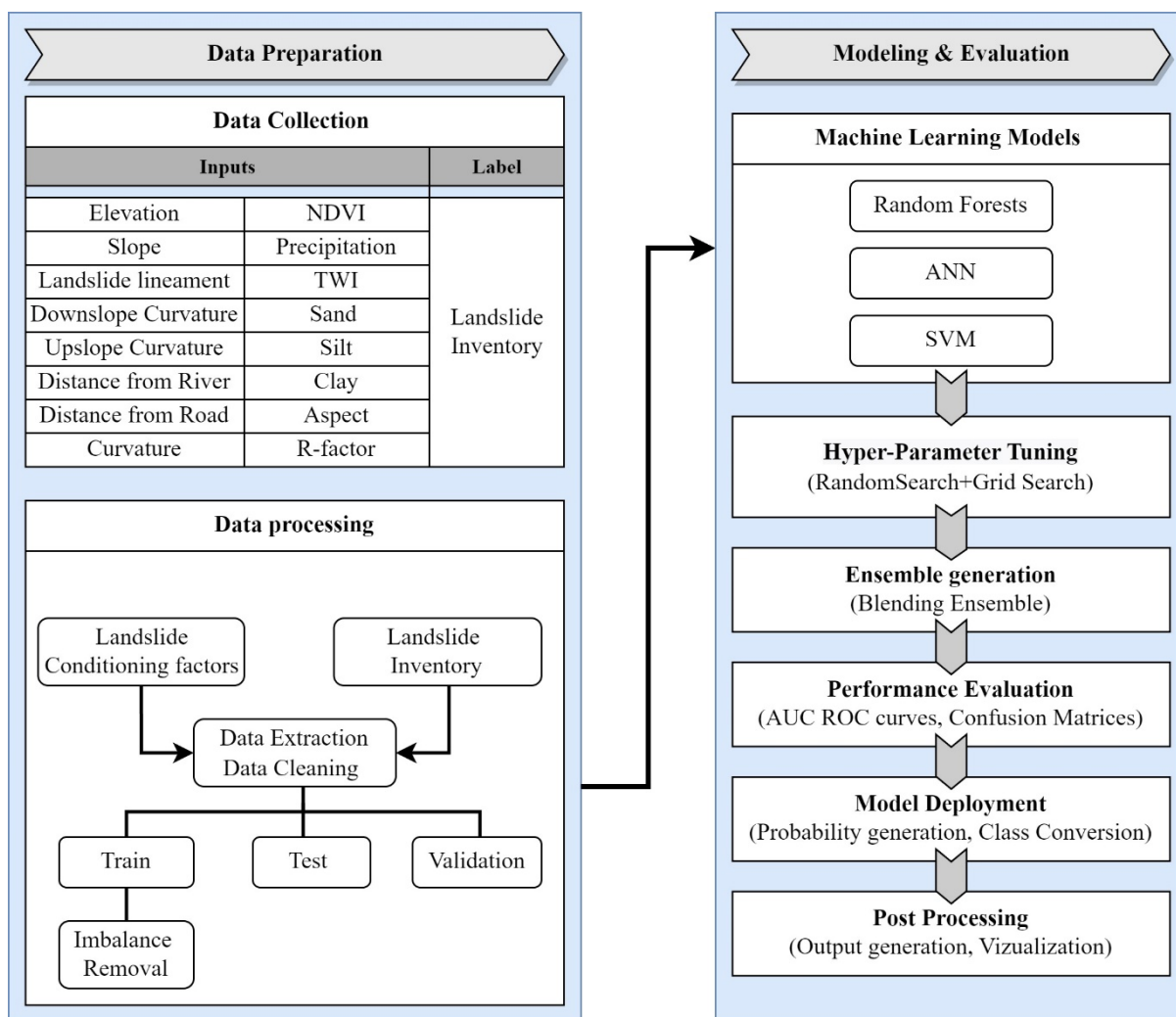
342

343   Figure 2 Methodology for developing a high-resolution landslide susceptibility map

344 **4.1   Data Pre-processing**

345 All the landslide conditioning datasets are resampled to a spatial resolution of $0.001°$. There

346 are no missing data points for 10 variables, and the missing data points for the rest of the 6

347 variables are less than 0.1% of the total data. The closest pixels in four directions are weighed

348 using inverse distance weighing to interpolate for the missing data points.

349 ### 4.1.1 Data Encoding

350 All the variables except the aspect are in numerical format. We need to convert the categorical

351 aspect values into numerical features to be used as input for machine learning models. We

352 benchmark multiple encoding methods like one-hot encoding, leave-one-out encoding, James

353 Stein encoding, mean encoding, and catboost encoding using a subset of landslide data. Based

354 on the results, James Stein encoding (Stein, 1956) is selected for encoding aspect.

355 ### 4.1.2 Data Split and normalization

356 If any landslide point lies inside the pixel, the pixel is assumed to be a landslide pixel. In the

357 case of landslide polygons, the polygons are first separated into training, testing, and validation

358 polygons and then transformed into pixels; this is important because neighborhood pixels of a

359 single polygon might be separated into the training and validation set causing the model

360 estimates to be over-optimistic (Emberson et al., 2021; Peña and Brenning, 2015). The testing

361 data and validation data non-landslide pixels are randomly sampled from the entire database

362 such that they are representative of the total data. After splitting, the datasets are scaled between

363 0-1 using a min-max scaler. Data normalization is done after splitting the data into training,

364 validation, and testing data to prevent data leakage.

365 ## 4.2 Imbalance handling of training data

366 Machine learning algorithms for classification are designed around the assumption of equal

367 data for all classes. However, since landslides are localized and rare event, the landslide

368 database is highly imbalanced. The number of data points representing the occurrence of

369 landslides is significantly lower than those representing non-occurrence of landslides.

370   Even the most common performance metrics, such as accuracy, assume balanced class

371   distribution. In case of imbalanced data, these algorithms lead to poor predictive performance,

372   especially for minority classes which are more important since multiple highly susceptible

373   landslide points identified as low susceptibility would degrade the usability of the model. A

374   machine learning model trained on unbalanced data will exhibit poor predictive performance,

375   especially in the case of landslide pixels, since it tends to be overfitted and biased towards non-

376   landslide points. Therefore, we remove the imbalance only from the training data. As explained

377   in section 4.1.2, the validation and testing data are supposed to be a subset of the original data

378   without including synthetic data; hence no imbalance removal techniques are applied to the

379   testing and validation data.

380   A simple way to deal with class imbalance is to resample the original data into balanced data

381   representative of the overall problem. Resampling includes oversampling the minority class or

382   undersampling the majority class. Undersampling means reducing the number of data points in

383   the majority class. Undersampling can be done by randomly removing the data points from the

384   majority class, also known as random undersampling. However, random undersampling has

385   the disadvantage of discarding potentially useful information essential for the model. To be

386   more discerning regarding the deletion of the majority class sample, a learning model should

387   be trained to identify redundant examples for deletion. In this study, we use One-Sided

388   Selection (OSS) technique to reduce most data points (Kubat and Matwin, 1997). OSS first

389   uses Tomek Links to reduce the number of ambiguous data points in the class boundary, and

390   then it uses Condensed Nearest Neighbours (CNN) to remove redundant data points far from

391   the class boundary. This method reduces the redundant data points from the majority class

392   significantly.

393   Oversampling data means increasing the number of data points in the minority class. Random

394   oversampling can be easily done by replicating the data points multiple times. Since similar

395 data points are repeated in random oversampling, this technique leads to the overfitting of the

396 model. A model fitted with random oversampling has high training accuracy but low testing

397 accuracy.

398 There are several approaches to informed oversampling, out of which Synthetic Minority

399 Oversampling Technique (SMOTE) is the most widely used (Chawla et al., 2011). SMOTE

400 randomly selects an example from the minority class and identifies k nearest neighbors of that

401 sample. A random nearest neighbor is then selected, and a line segment is drawn between the

402 example and the selected nearest neighbor; a synthetic example is then created at a random

403 point between the line. This method can be used to generate any number of synthetic samples.

404 SMOTE creates synthetic instances without considering the majority class, which might result

405 in incorrect synthetic data if the majority and minority classes overlap. Hence, we also compare

406 multiple extensions of SMOTE that consider the decision boundary to generate synthetic

407 samples. The Borderline-SMOTE1 (BLSMOTE) (Han et al., 2005) can generate samples near

408 the decision boundary. The SVMSMOTE (Nguyen et al., 2011) uses an SVM classifier on the

409 original dataset to create a decision boundary and then creates synthetic samples along lines

410 joining the minority class support vector and the data points. The Adaptive Synthetic Sampling

411 Approach (ADASYN) (He et al., 2008) creates synthetic samples that are inversely

412 proportional to the density of the minority class examples. All these approaches are compared

413 using fivefold cross-validation on raw landslide data using Random Forests Classifier and

414 accuracy as a metric. SVMSMOTE has the highest oversampling accuracy, whereas random

415 oversampling has the lowest accuracy. The combination of undersampling and oversampling

416 methods improves the overall performance of machine-learning models (Chawla et al., 2011).

417 Since the data imbalance in the case of landslides is extremely high, we firstly use OSS to

418 undersample the data and SVMSMOTE to oversample the data to create an accurate

419 representation of the entire dataset and enhance the performance of machine learning models.

420   The combination of undersampling and oversampling makes the model more robust. In the

421   case of large datasets, it reduces the majority class significantly, thereby reducing the total data

422   required for model training.

423   **4.3   Machine learning based modelling**

424   Machine learning based classification methods map the interactions between the various input

425   datasets to the label data to model the underlying fundamental processes. For modelling a

426   spatially heterogenous area such as India with multiple landslide types, it is critical to use

427   approaches that do not assign apriori weights to input parameters (Emberson et al., 2021).

428   There is a growing preference for machine learning methods to avoid arbitrary

429   parameterization (Reichenbach et al., 2018; Ahmed et al., 2020; Youssef and Pourghasemi,

430   2021). Machine Learning models such as Support Vector Machines (Pham et al., 2016b;

431   Pradhan, 2013), Random Forests (Chen et al., 2018; Emberson et al., 2021), XGBoost

432   (Kavzoglu and Teke, 2022), ANN (Hong et al., 2020) have been extensively used in landslide

433   studies. Ensemble models that combine information from individual models to generate a more

434   robust and accurate final model have recently been used for landslide studies (Pham et al.,

435   2017; Felsberg et al., 2021).

436   The machine learning classifiers used in this study are discussed below.

437   4.3.1   Random Forest classifier

438   The idea behind bagging is that by training multiple models on different subsets of the data,

439   each model will be able to learn from different variations in the data. Bagging classifiers use a

440   random subset of the dataset with replacement to train various weak models. The majority

441   voting aggregates these final predictions of all weak models, thereby reducing the model's

442   variance, which can improve the model's ability to generalize to new data making more

443   accurate predictions. We use Random Forest model (Breiman, 2001), where bagging is used to

444 train various decision tree models. The trees are independent of each other and have equal

445 weightage in the final output. Since each dataset is randomly sampled, Random Forest has a

446 higher variance and low bias than Decision Trees.

447 4.3.2   Artificial Neural Networks

448 Artificial Neural Network (ANN) is a machine learning model inspired by the brain's neural

449 pathways. ANNs are interconnected nodes that receive input from other neurons and then

450 process the input using an activation function. The output is then passed on to other neurons in

451 the network. The strength of the connections between the neurons, called weights, which

452 determines the importance of the input received by each neuron. The weights are adjusted

453 during the learning process by the training data. We use feedforward neural networks with a

454 backpropagation algorithm. The neural network has rectified linear units as activation functions

455 and Adam optimizer.

456 4.3.3   SVM classifier

457 The SVM classifier assumes that data not linearly separable will become linearly separable if

458 transformed into a higher dimension. The transformation of data into higher dimension is done

459 using a kernel function. SVM uses the transformed data to define the decision boundary known

460 as a hyperplane (Cortes and Vapnik, 1995). SVMs have several advantages, including high

461 accuracy, the ability to handle high-dimensional data, and the ability to perform well on small

462 datasets. However, they are computationally intensive because their time complexity increases

463 more than quadratically. Hence with large samples, it becomes difficult to scale. This study

464 uses an SVM classifier with a radial basis function to define a hyperplane.

465 **4.4   Hyperparameter Tuning**

466 Machine learning models learn the model parameters when provided with training data.

467 Hyperparameters, on the other hand, are a set of external parameters of a model that decide the

22

468   model's architecture and are not derived from data. Hyperparameters are set before training the

469   model and vary from model to model. To identify the hyperparameters, we use coarse to fine-

470   tuning, which uses random search in collaboration with grid search to find the optimal set of

471   hyperparameters. This methodology aids in the discovery of hyperparameters while incurring

472   the least amount of computational expense. Firstly, a random search narrows the range for each

473   hyperparameter, followed by a grid search to precisely specify and assess the parameter

474   combination. In the case of random forests, we use maximum tree depth, number of estimators,

475   and maximum features as hyperparameters. In the case of the SVM kernel, the function is kept

476   as a radial basis function, and C and gamma hyperparameters are used for tuning. For ANN,

477   we vary the number of neurons and hidden layers to find the optimum architecture.

478   **4.5   Ensemble Machine Learning**

479   Ensemble machine learning fuses the results of individual models to enhance the overall

480   predictability and robustness. Ensemble machine learning works best when individual models

481   are not only accurate but also diverse i.e vulnerable to different kinds of noise. In this study

482   after developing multiple models, we select SVM, ANN, and Random forest for ensemble

483   generation since they were not only highly accurate are based on different underlying

484   principles. Traditional methodologies, such as the average and weighted average rules, can be

485   used to build ensembles, but these tactics are overly simplistic and may not be as accurate,

486   therefore, newer techniques, such as stacking are becoming more prominent. Stacking

487   optimally combines the results of multiple classifiers, also known as base classifiers, using a

488   meta classifier. Stacking uses k-fold cross-validation of the training data, the base models are

489   trained on k-1 folds, whereas the meta-model is trained on out-of-fold predictions. We use a

490   case of stacking ensemble known as blending ensemble where initial training data is split into

491   base model training and meta-model validation data; this leads to less information leakage than

492   a stacking ensemble. The blending ensemble has been found to outperformed stacking,

493   averaging and weighted averaging of machine learning and deep learning models for landslide

494   susceptibility mapping (Fang et al., 2021).

495   In this study, we create a blending ensemble using SVM, ANN, and Random Forest models as

496   base level models and Logistic Regression as the meta-model. The base level models have

497   different underlying principles; therefore, the ensemble model is free from the biases of a single

498   model, making the ensemble more robust. Since the aim of meta model in a blending ensemble

499   is to optimally combine the outputs of the base model, hence we use a simple meta model

500   without hyperparameter tuning of meta model parameters. Using a complex meta model and

501   hyperparameter tuning would require additional computation power as well as additional data

502   split without adding much information to model.

503   **4.6   Model Validation**

504   The testing data must be randomly sampled from the overall dataset. Since the overall dataset

505   is highly imbalanced, the testing data will also be imbalanced. The techniques like

506   undersampling and oversampling change the overall data structure, therefore, they cannot be

507   applied for testing. The final dataset had total of 1282908 data points with 641454 of landslide

508   and non-landslide points. The testing data contains randomly sampled 15000 landslide points

509   and 300000 non-landslide points.

510   The metrics used to test the accuracy of our model are explained below:

511   a) The Area Under the Receiver Operating Characteristic curve (AUCROC) indicates how

512   well the model predicts 0 values as 0 and 1 value as 1. When presented with imbalanced

513   data sets, AUCROC cannot give an accurate picture of the skill of the classifier;

514   therefore, it is used in conjunction with other methods to evaluate model efficacy.

515   b)   Accuracy is the ratio of correct predictions to total predictions and is an overall metric

516   to check how well the model can differentiate between classes. Accuracy works well

517   only in cases where positive samples are equal to negative ones.

518   c)   Sensitivity is the rate of positivity and is the ratio of True Positives to the total number

519   of positive samples. Sensitivity is the most important metric in the case of landslides

520   classification as it shows the model's capability to identify the existence of landslides

521   (True Positives) since a landslide prone area classified as a low probability is much

522   worse than an area without landslides being classified as landslide susceptible.

523   d)   Precision is the ratio of True Positives and total data points classified as positives.

524   Precision shows the ability of the model to identify relevant data points from total data

525   points.

526   e)   Matthews correlation or MCC is a reliable measure based on the mean square

527   contingency coefficient that produces a high score only if the prediction performs well

528   in all four confusion matrix categories and is used to check the overall model

529   performance, which is crucial for imbalanced datasets.

530   4.7   Output generation

531   After completing the training, validation, and testing of individual machine learning models

532   and the ensemble model, the ensemble model to estimate the probability of landslide for each

533   pixel. These probabilities lie between 0 to 1 and are treated as a quantitative estimate of

534   susceptibility. These values are transformed into a single metric of susceptibility classes using

535   Jenks natural breaks classification method. Jenks method has been widely used for landslide

536   susceptibility classification from landslide probability (Piacentini et al., 2012; Sterlacchini et

537   al., 2011). The Jenks method finds optimal class breaks by minimizing the sum of the squared

538   deviations within each class, thereby minimizing inter-class variance and maximizing intra-

539   class variance.

540   **5   Results**

541   **5.1   Accuracy metrics**

542   The ensemble model outperforms all individual machine learning models. Figure 3 (a) shows

543   the AUC ROC curve of individual models and the ensemble. The normalized confusion matrix

544   for the ensemble model is shown in Figure 3 (b). Due to a high imbalance in the testing data,

545   the metrics will be highly skewed towards non-landslide points if a normal confusion matrix is

546   used. On the other hand, a normalized confusion matrix transforms the values such that the

547   sum of each row is 1, thus giving a more accurate representation of the model performance for

548   imbalanced data.

549

550
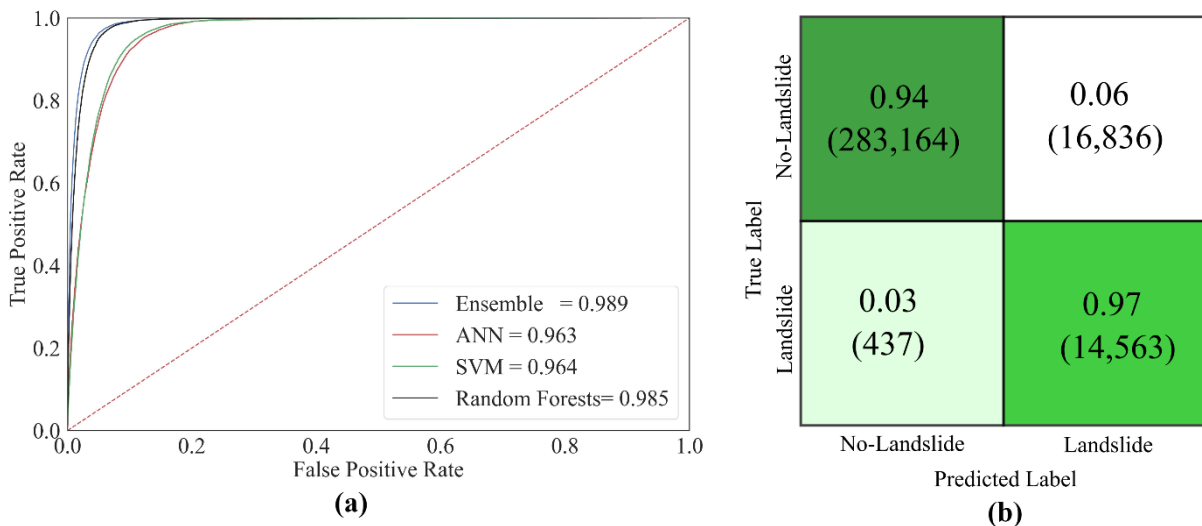
551

552   Figure 3 (a) AUCROC curves for individual machine learning models and blended ensemble

553   model (b) Normalized Confusion Matrix for the ensemble model

26

554 Sensitivity, precision, and Matthew's correlation coefficient are derived from the confusion

555 matrices to ascertain the skill of the models and are shown in Table 3. The ensemble model

556 performs well in all spheres and has the highest accuracy, sensitivity, precision and MCC than

557 the individual models showcasing the superiority of ensemble based model.

558 Table 3 Accuracy metrics for various models

Metric	Expression	Random Forests	SVM	ANN	Ensemble
Accuracy	$\dfrac{TP + TN}{TP + TN + FP + FN}$	95.24	91.58	90.90	95.73
Sensitivity	$\dfrac{TP}{TP + FN}$	96.21	92.46	91.62	97.08
Precision	$\dfrac{TP}{TP + FP}$	94.39	90.86	90.31	94.53
Matthews Correlation	$\dfrac{TP * TN - FP * FN}{\sqrt{(TP + FP)(TP + FN)(TN + FP)(TN + FN)}}$	0.905	0.831	0.818	0.915

559

5.2 Relative importance of landslide conditioning factors

561 Figure 4 shows the feature importance of the Random Forests model, which indicates the

562 predictive potential of individual landslide conditioning factors. All the input variables

563 contribute to the model development since the redundant variables are removed during model

564 development using feature selection. The slope, TWI, and elevation have the highest feature

565 importance value for the Random Forest model. India's newly developed road database also

566 contributes highly to the model since many landslides in hilly areas are detected along the

567 roadside. The erosivity factor, although a less used landslide conditioning factor, has high

568 feature importance, indicating that it should be incorporated in regional landslide prediction

569 models and developed at high spatial resolution.
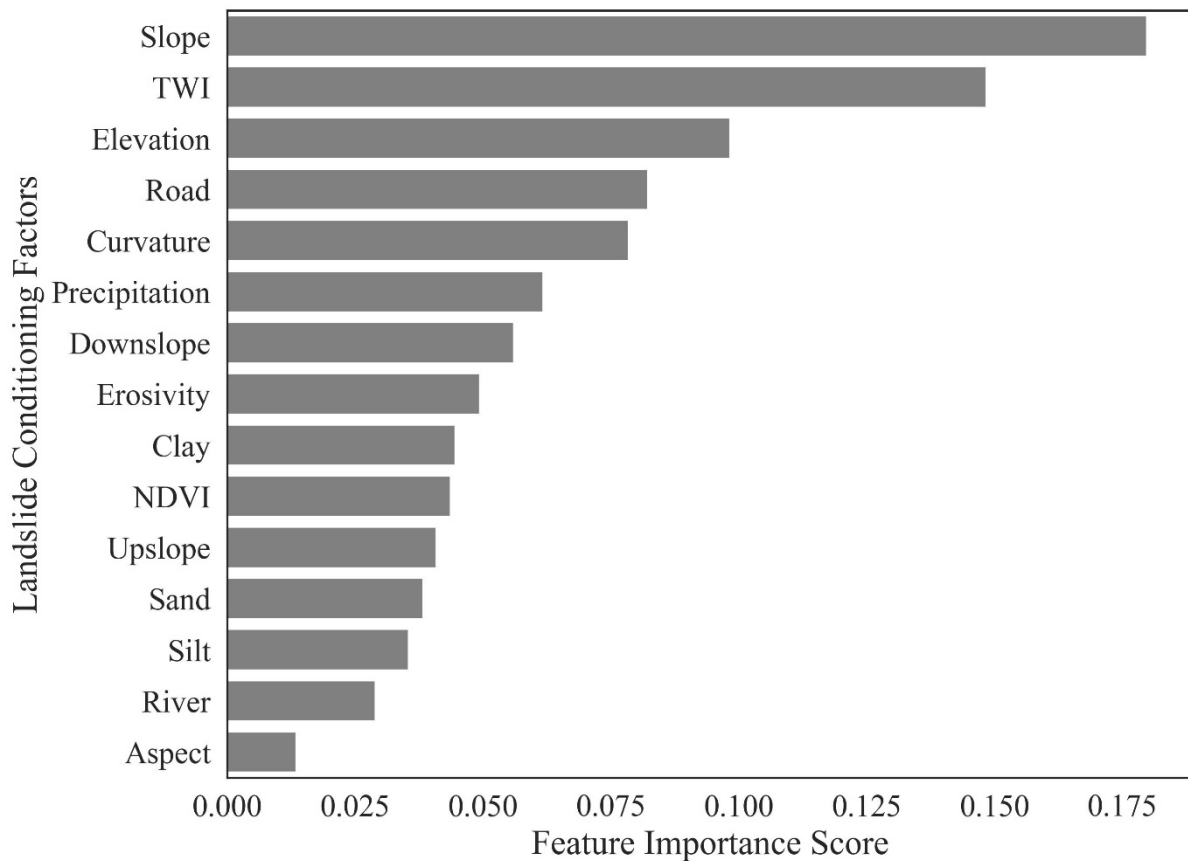
Figure 4 Feature Importance using Random Forest model

5.3   Developing the India Landslide Susceptibility Map (ILSM)

573   The India Landslide Susceptibility Map is developed by dividing the ensemble landslide

574   probability into 5 susceptibility classes according to the procedure described in section 4.7.

575   The landslide susceptibility map is transformed into five classes, namely Very Low

576   (probability <= 0.1), Low (0.10<probability<=0.30), Medium (0.30<probability<=0.54),

577   High (0.54<probability<=0.78), Very High (probability > 0.78). Figure 5 shows the India

578   Landslide Susceptibility Map (ILSM).
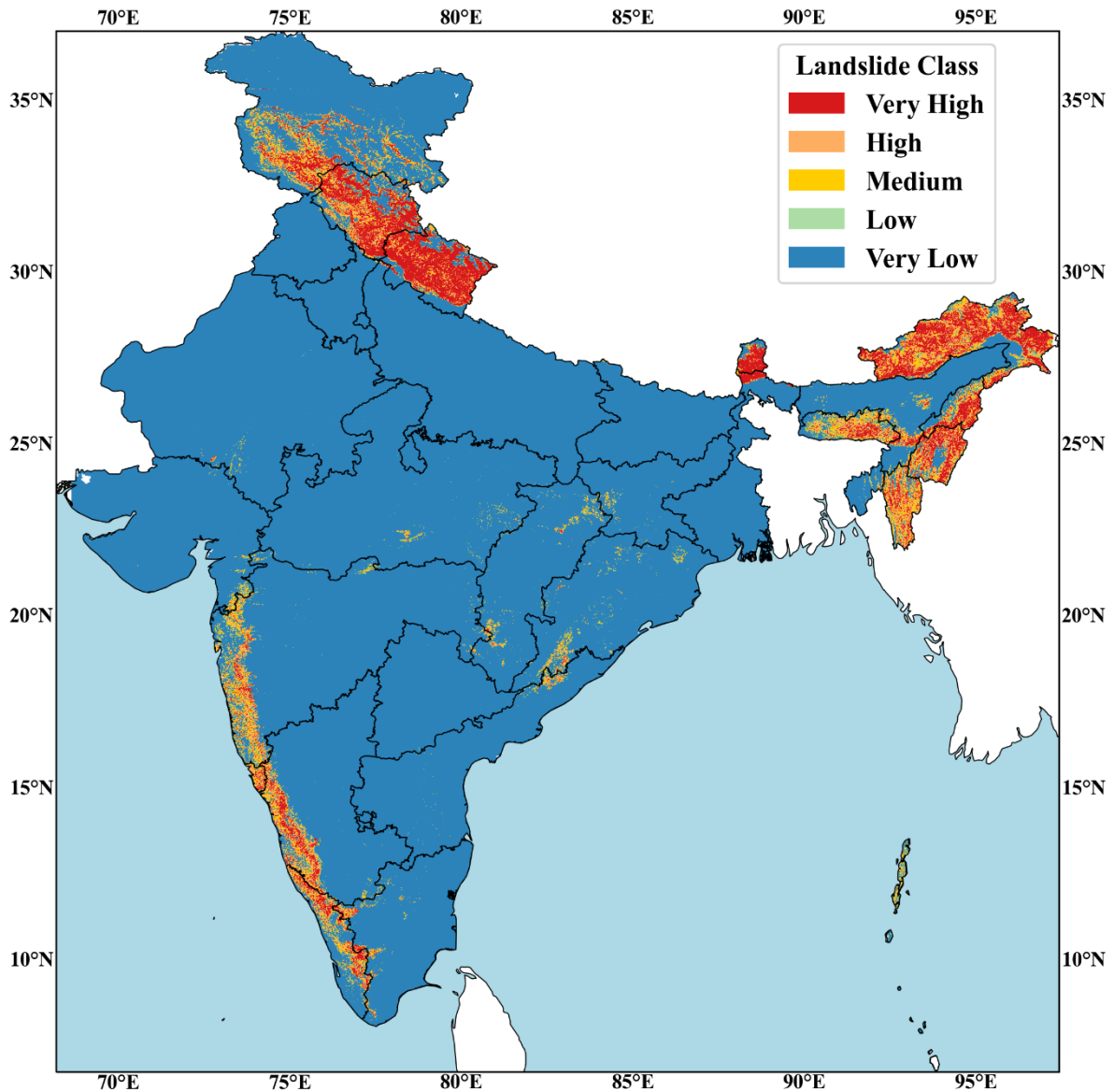
579

580   Figure 5 India Landslide Susceptibility Map (ILSM)

581   Table 4 Distributions of landslide percentage by class.

Landslide Susceptibility Class	Area in percentage
Very High	4.745
High	3.529
Medium	3.196
Low	1.694
Very Low	86.835

582

583   Table 4 shows the distribution of landslide susceptibility by class. The India Landslide

584   susceptibility map shows that 4.745% of India is very highly susceptible to landslides. The

585   ILSM shows that the total area susceptible to landslides is 13.17%, whereas the Geological

586   Survey of India estimates that around 12.6% area of India is susceptible to landslides. The top

587   10 landslide susceptible states in India, according to ILSM, are shown in Figure 6. The

588   Himalayas are the most affected due to landslides often associated with heavy rainfall. The

589   Western Ghats, characterized by steep slopes and thick soil cover is India's second most

590   landslide-affected region. Figure 6 shows state wise distribution of landslide susceptibility.

591   Sikkim has the highest percentage land area (57.6%) susceptible to landslides, whereas

592   Arunachal Pradesh, 31845 km2, has the highest area susceptible to landslides. Among the non-

593   Himalayan regions, Kerala has the highest area susceptible to landslides, with 14.32% in the

594   very high susceptibility zone and 15.73% in the high susceptibility zone.
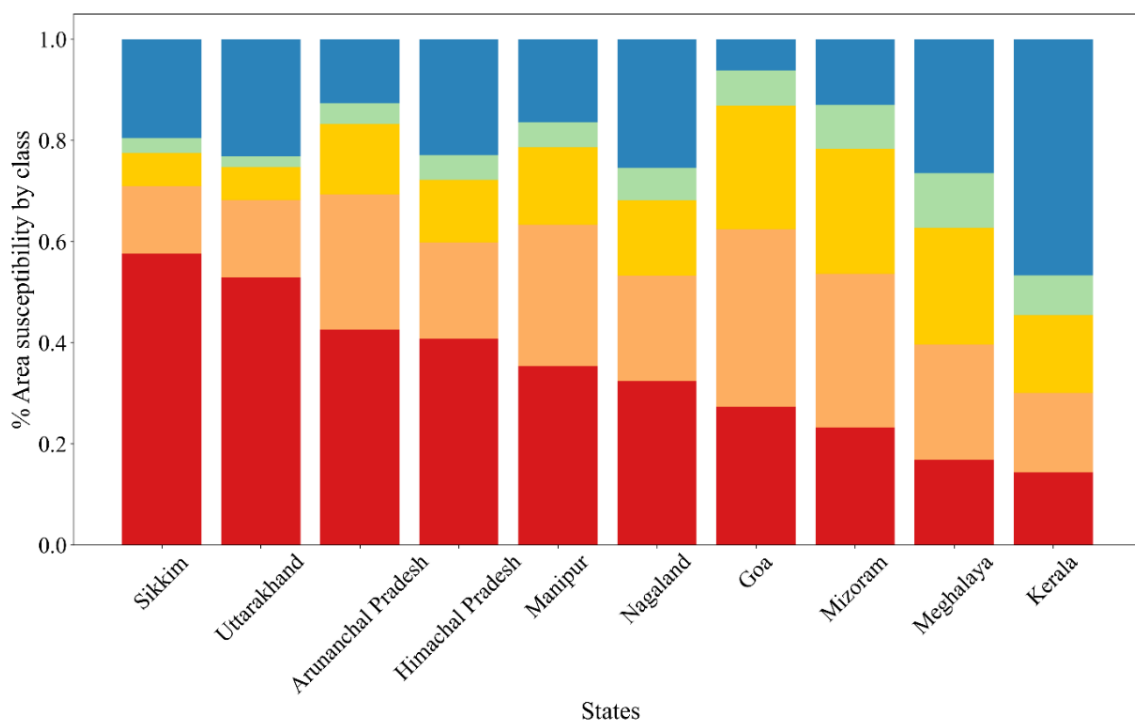
595

596   Figure 6 Top 10 landslide susceptible states in India (by the percentage of area)

597   **5.4   Newly Identified Landslide Zones**

598   The current ILSM and NLSM identify similar areas as highly susceptible to landslides, but

599   ILSM identifies a larger landslide susceptible area, especially in the eastern ghats, as shown in

600   Figure 7.

601
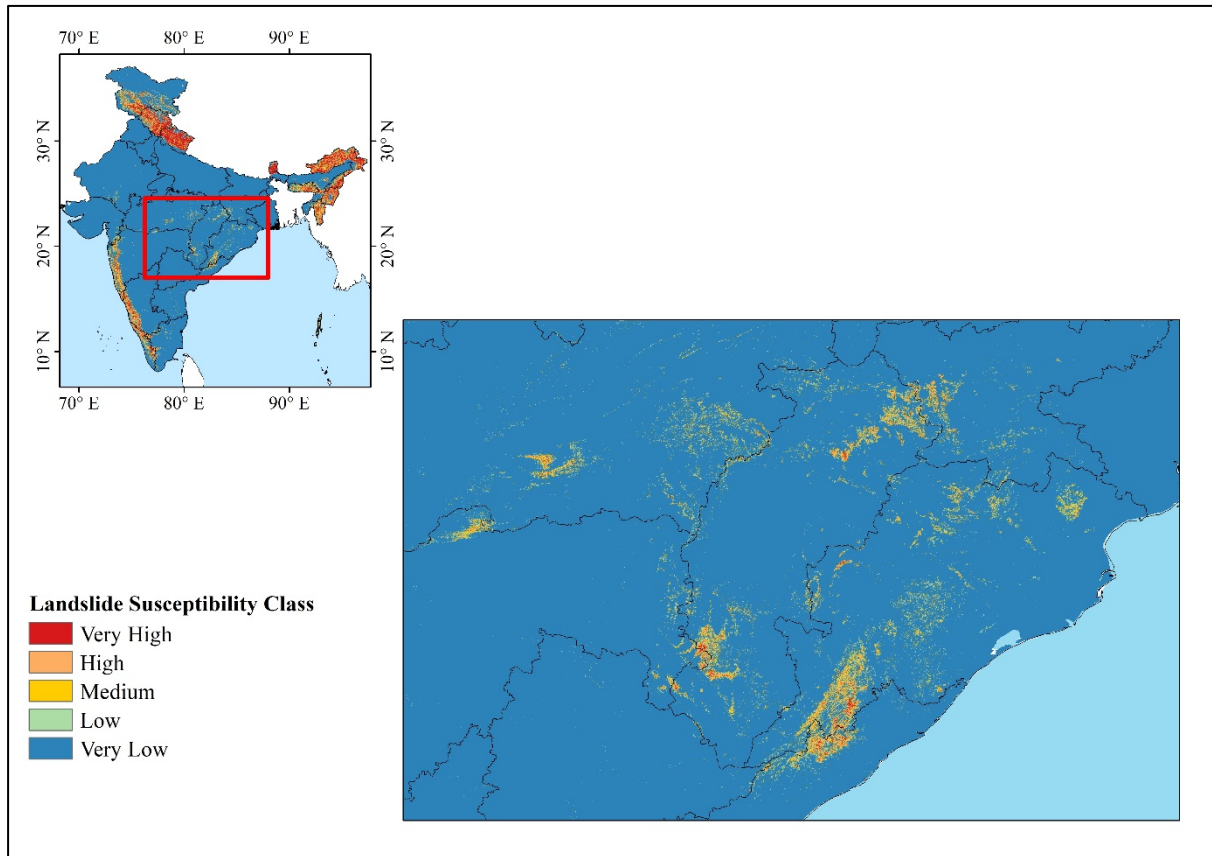
602   Figure 7 Newly identified medium landslide susceptibility zones in eastern ghats

603   The presence of landslides in the eastern ghats is further validated using other global landslide

604   inventories (Froude and Petley, 2018). The identification of new landslide regions by ILSM

605   highlights the superiority of the methodology presented in this study and the inherent advantage

606   of machine learning based frameworks to learn meaningful information about landslide

607   conditioning factors from other areas with similar conditions. Additionally, this map points

608   towards the need for a thorough study with an updated landslide inventory to understand the

609   landslides' behavior in the eastern ghats.

31

5.5   Comparison with an independent landslide inventory

To assess the quality of our framework and demonstrate the reliability of the ILSM, we compare the final landslide susceptibility map results with an independent landslide inventory, the global fatal landslide database (Froude and Petley, 2018) which contains fatal landslides recorded between 2001-2017. Figure 8 shows the locations of landslides and their corresponding landslide susceptibility class according to ILSM. Most of the landslides fall in the very high landslide category. Global fatal landslide catalogue also shows some landslide in the eastern ghats region in line with ILSM. Although there are some landslides in very low category they are rare and localized to a few events.
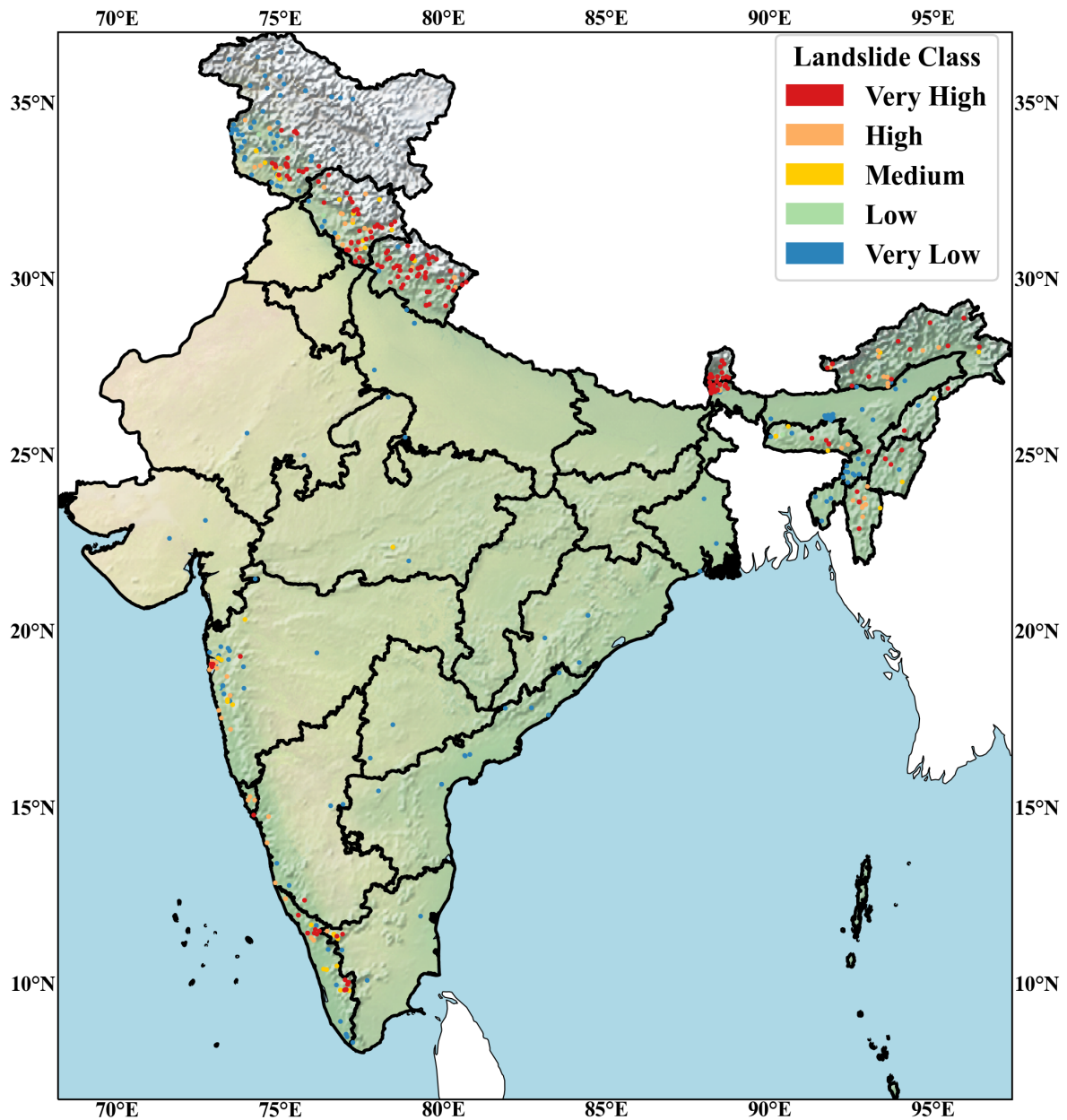
Figure 8 Location of global fatal landslides database by ILSM class

6　Discussion

In this study, we have developed a comprehensive framework for high resolution landslide

susceptibility mapping using a combination of multiple machine learning models. We use the

framework to develop a pan-India landslide susceptibility map.

This study improves upon the earlier reported studies by:

626   a. Embracing big data: Rather than using coarse resolution data, we use big data to

627   consider the spatiotemporal heterogeneity which enables our machine learning model

628   to generalize and produce accurate landslide susceptibility map. Most of the landslide

629   research is based on limited landslide inventories which makes it challenging to develop

630   data driven models. This study employs 154,329 landslide points in a national landslide

631   inventory meticulously mapped by GSI and 489 landslide points from the global

632   landslide repository. Additionally, we also move away from random sampling

633   techniques towards sophisticated resampling techniques to create a representative and

634   balanced training dataset for the machine learning models.

635   b. Ensemble methodology: A single machine learning model is based on a single principle

636   and can produce inaccurate results for specific cases. In this study, we use an ensemble

637   of multiple machine learning models with different underlying principles, making our

638   model more robust and freer from individual model bias.

639   c. Improved input data: Machine learning techniques heavily depend on input data quality

640   (Geiger et al., 2020). In this study, we used a combination of Earth observation data

641   with ground data to generate India Landslide Susceptibility Map (ILSM). We utilize

642   the improved MERIT DEM in conjunction with national datasets for roads and rivers,

643   which have been ground mapped extensively under the directive of the Government of

644   India and significantly improve upon the previous datasets. We also use rainfall kinetic

645   energy (rainfall erosivity) and TWI data, which are often overlooked in landslide

646   susceptibility studies; these datasets are found to significantly contribute to the model.

647   d. Identifies new landslide zones: This study identifies a much larger area is susceptible

648   to landslides especially in the eastern ghats, which is not considered for developing

649   landslide susceptibility in India's official landslide susceptibility map NLSM.

650 e. Usability: The explicit landslide probability and class provided in this study can be used

651 for prioritizing landslide research, studying compound hazards, and understanding the

652 impact of landslides on the environment. Comprehensive landslide susceptibility maps

653 can help policy makers to design effective mitigation measures against landslides.

7   Conclusion

Every year landslides claim many lives and cause losses amounting to billions of dollars. Understanding the areas prone to landslides and the factors driving them is critical to reducing the impact of landslides. This study aims to develop a framework that leverages big data and uses state of the art data curation and machine learning methods to map landslides at a high spatial resolution. Machine learning models are flexible on datasets and resolution, therefore the framework suggested in this study can be implemented on a variety of datasets, given the datasets are consistent. This methodology is especially useful in developing and underdeveloped countries where ground datasets are absent and landslide models are based on earth observation data. The framework also provides ensemble probabilistic estimates for landslide susceptibility which can help develop landslide models. Using the framework, we develop the India Landslide Susceptibility Map which is not only able to replicate the landslide zones identified in the existing national and global maps but is also able to identify new landslide zones. The ILSM can therefore be used for awareness of present and future landslide hotspots, prioritization of future landslide research, and designing development strategies in the landslide prone regions. However, in this methodology all types of rainfall induced landslides are considered equivalent, but in the real world, the factors driving landslides are more complex. To understand how a machine learning frameworks model different kinds of landslides spatially as well as by type requires an extensive study using local model interpretation methods. Another important factor in machine learning based studies is the quality of input datasets. Most the datasets used in this study are developed using remote sensing which is susceptible to sensor and calibration noise. Therefore, an improvement in input datasets can help improve machine learning based landslide susceptibility maps further. Also, an area where landslides are more frequent is more susceptible to landslides than an area with a single landslide. These shortcomings will be a subject for future research. The products of this study are freely available in google earth engine.

685 for this research through ISRO Space Applications Center (RP04139). This work was also

686 supported by the IIT Delhi IoE funded project (PLN12/02CE). The authors gratefully

687 acknowledge the Geological Survey of India (GSI) and Pradhan Mantri Gram Sadak Yojana

688 (PMGSY) for the datasets used in this study. The authors acknowledge the IIT Delhi High

689 Performance Computing facility for providing computational and storage resources.

690 **Data Availability**

691 The Indian Landslide Susceptibility Map (ILSM) probability and class data is freely available

692 from

693 1) Raw Tiff files

694 • ILSM probability https://bit.ly/3ibptIP

695 • ILSM class https://bit.ly/3IidXGn

696 2) Google Earth engine:

697 • var ILSM_class= ee.Image("projects/ee-nirdeshsharmanith1/assets/ILSM")

698 • var ILSM_probability=ee.Image("projects/ee-

699 nirdeshsharmanith1/assets/ILSM_probability")

700 3) Code: https://github.com/hydrosenselab/ILSM

701 **References:**

702 Ahmad, A., Lopulisa, C., Imran, A., Baja, S., 2019. Rainfall erosivity in climate changes and
703   the connection to landslide events, in: IOP Conference Series: Earth and Environmental
704   Science. p. 012007. https://doi.org/10.1088/1755-1315/280/1/012007
705 Ahmed, N., Firoze, A., Rahman, R.M., 2020. Machine learning for predicting landslide risk of
706   Rohingya refugee camp infrastructure. J. Inf. Telecommun. 4, 175–198.
707   https://doi.org/10.1080/24751839.2019.1704114
708 Alimohammadlou, Y., Najafi, A., Yalcin, A., 2013. Landslide process and impacts: A proposed
709   classification method. CATENA 104, 219–232.
710   https://doi.org/10.1016/j.catena.2012.11.013
711 Anbalagan, R., Singh, B., 1996. Landslide hazard and risk assessment mapping of mountainous
712   terrains — a case study from Kumaun Himalaya, India. Eng. Geol. 43, 237–246.
713   https://doi.org/10.1016/S0013-7952(96)00033-6

Azarafza, Mohammad, Azarafza, Mehdi, Akgün, H., Atkinson, P.M., Derakhshani, R., 2021. Deep learning-based landslide susceptibility mapping. Sci. Rep. 11, 24112. https://doi.org/10.1038/s41598-021-03585-1

Bălteanu, D., Chendeş, V., Sima, M., Enciu, P., 2010. A country-wide spatial assessment of landslide susceptibility in Romania. Geomorphology, Recent advances in landslide investigation 124, 102–112. https://doi.org/10.1016/j.geomorph.2010.03.005

Breiman, L., 2001. Random Forests. Mach. Learn. 45, 5–32. https://doi.org/10.1023/A:1010933404324

Bureau of Indian Standards, 1998. IS 14496-2: Guidelines for preparation of landslide - Hazard zonation maps in mountainous terrains, Part 2: Macro-zonation.

Castellanos Abella, E.A., Van Westen, C.J., 2008. Qualitative landslide susceptibility assessment by multicriteria analysis: A case study from San Antonio del Sur, Guantánamo, Cuba. Geomorphology, GIS technology and models for assessing landslide hazard and risk 94, 453–466. https://doi.org/10.1016/j.geomorph.2006.10.038

Cellek, S., 2021. The Effect of Aspect on Landslide and Its Relationship with Other Parameters, in: Landslides. IntechOpen. https://doi.org/10.5772/intechopen.99389

Chang, K.-T., Merghadi, A., Yunus, A.P., Pham, B.T., Dou, J., 2019. Evaluating scale effects of topographic variables in landslide susceptibility models using GIS-based machine learning techniques. Sci. Rep. 9, 12296. https://doi.org/10.1038/s41598-019-48773-2

Chawla, N.V., Bowyer, K.W., Hall, L.O., Kegelmeyer, W.P., 2011. SMOTE: Synthetic Minority Over-sampling Technique. https://doi.org/10.48550/ARXIV.1106.1813

Chen, W., Peng, J., Hong, H., Shahabi, H., Pradhan, B., Liu, J., Zhu, A.-X., Pei, X., Duan, Z., 2018. Landslide susceptibility modelling using GIS-based machine learning techniques for Chongren County, Jiangxi Province, China. Sci. Total Environ. 626, 1121–1135. https://doi.org/10.1016/j.scitotenv.2018.01.124

Compendium of Task Force Sub Group Reports on National Landslide Risk Management Strategy (https://www.ndma.gov.in/sites/default/files/PDF/Landslide/Compendium-NLRMS.pdf), 2019.

Cortes, C., Vapnik, V., 1995. Support-vector networks. Mach. Learn. 20, 273–297.

CRED, 2022. . Centre for Research on the Epidemiology of Disasters (CRED).

Dinanta, G.P., Cassidy, D.P., Octariady, J., Fernando, D., Yusuf, M.D., 2020. Assessing landslide susceptibility using ANN and ANFIS to forecast landslides in Sumatera Indonesia, in: 2020 IEEE Asia-Pacific Conference on Geoscience, Electronics and Remote Sensing Technology (AGERS). Presented at the 2020 IEEE Asia-Pacific Conference on Geoscience, Electronics and Remote Sensing Technology (AGERS), pp. 1–11. https://doi.org/10.1109/AGERS51788.2020.9452781

Emberson, R.A., Kirschbaum, D.B., Stanley, T., 2021. Landslide Hazard and Exposure Modelling in Data-Poor Regions: The Example of the Rohingya Refugee Camps in Bangladesh. Earths Future 9, e2020EF001666. https://doi.org/10.1029/2020EF001666

Fang, Z., Wang, Y., Peng, L., Hong, H., 2021. A comparative study of heterogeneous ensemble-learning techniques for landslide susceptibility mapping. Int. J. Geogr. Inf. Sci. 35, 321–347. https://doi.org/10.1080/13658816.2020.1808897

Felsberg, A., Poesen, J., Bechtold, M., Vanmaercke, M., De Lannoy, G.J.M., 2021. Estimating global landslide susceptibility and its uncertainty through ensemble modelling. Nat. Hazards Earth Syst. Sci. Discuss. 1–30. https://doi.org/10.5194/nhess-2021-360

Fick, S.E., Hijmans, R.J., 2017. WorldClim 2: new 1-km spatial resolution climate surfaces for global land areas. Int. J. Climatol. 37, 4302–4315. https://doi.org/10.1002/joc.5086

Froude, M.J., Petley, D.N., 2018. Global fatal landslide occurrence from 2004 to 2016. Nat. Hazards Earth Syst. Sci. 18, 2161–2181. https://doi.org/10.5194/nhess-18-2161-2018

Gaidzik, K., Ramírez-Herrera, M.T., 2021. The importance of input data on landslide susceptibility mapping. Sci. Rep. 11, 19334. https://doi.org/10.1038/s41598-021-98830-y

Gaprindashvili, G., Van Westen, C.J., 2016. Generation of a national landslide hazard and risk map for the country of Georgia. Nat. Hazards 80, 69–101. https://doi.org/10.1007/s11069-015-1958-5

Geiger, R.S., Yu, K., Yang, Y., Dai, M., Qiu, J., Tang, R., Huang, J., 2020. Garbage In, Garbage Out? Do Machine Learning Application Papers in Social Computing Report Where Human-Labeled Training Data Comes From? Proc. 2020 Conf. Fairness Account. Transpar. 325–336. https://doi.org/10.1145/3351095.3372862

Gorelick, N., Hancher, M., Dixon, M., Ilyushchenko, S., Thau, D., Moore, R., 2017. Google Earth Engine: Planetary-scale geospatial analysis for everyone. Remote Sens. Environ. https://doi.org/10.1016/j.rse.2017.06.031

Günther, A., Van Den Eeckhaut, M., Malet, J.-P., Reichenbach, P., Hervás, J., 2014. Climate-physiographically differentiated Pan-European landslide susceptibility assessment using spatial multi-criteria evaluation and transnational landslide information. Geomorphology 224, 69–85. https://doi.org/10.1016/j.geomorph.2014.07.011

Guzzetti, F., Paola, R., Ardizzone, F., Cardinali, M., Galli, M., 2006. Estimating the quality of landslide susceptibility models. Geomorphology 81, 166–184. https://doi.org/10.1016/j.geomorph.2006.04.007

Han, H., Wang, W.-Y., Mao, B.-H., 2005. Borderline-SMOTE: A New Over-Sampling Method in Imbalanced Data Sets Learning, in: Huang, D.-S., Zhang, X.-P., Huang, G.-B. (Eds.), Advances in Intelligent Computing, Lecture Notes in Computer Science. Springer, Berlin, Heidelberg, pp. 878–887. https://doi.org/10.1007/11538059_91

He, H., Bai, Y., Garcia, E.A., Li, S., 2008. ADASYN: Adaptive synthetic sampling approach for imbalanced learning, in: 2008 IEEE International Joint Conference on Neural Networks (IEEE World Congress on Computational Intelligence). Presented at the 2008 IEEE International Joint Conference on Neural Networks (IEEE World Congress on Computational Intelligence), pp. 1322–1328. https://doi.org/10.1109/IJCNN.2008.4633969

Highland, L.M., Godt, J.W., Howell, D.G., Savage, W.Z., 1998. El Nino 1997-98; damaging landslides in the San Francisco Bay area. US Dept. of the Interior, US Geological Survey, National Landslide ….

Hijmans, R.J., Cameron, S.E., Parra, J.L., Jones, P.G., Jarvis, A., 2005. Very high resolution interpolated climate surfaces for global land areas. Int. J. Climatol. 25, 1965–1978. https://doi.org/10.1002/joc.1276

Hong, H., Tsangaratos, P., Ilia, I., Loupasakis, C., Wang, Y., 2020. Introducing a novel multi-layer perceptron network based on stochastic gradient descent optimized by a meta-heuristic algorithm for landslide susceptibility mapping. Sci. Total Environ. 742, 140549. https://doi.org/10.1016/j.scitotenv.2020.140549

Hong, Y., Adler, R., Huffman, G., 2007. Use of satellite remote sensing data in the mapping of global landslide susceptibility. Nat. Hazards 43, 245–256. https://doi.org/10.1007/s11069-006-9104-z

Juang, C.S., Stanley, T.A., Kirschbaum, D.B., 2019. Using citizen science to expand the global map of landslides: Introducing the Cooperative Open Online Landslide Repository (COOLR). PLOS ONE 14, e0218657. https://doi.org/10.1371/journal.pone.0218657

Kavzoglu, T., Teke, A., 2022. Predictive Performances of Ensemble Machine Learning Algorithms in Landslide Susceptibility Mapping Using Random Forest, Extreme Gradient Boosting (XGBoost) and Natural Gradient Boosting (NGBoost). Arab. J. Sci. Eng. https://doi.org/10.1007/s13369-022-06560-8

Kubat, M., Matwin, S., 1997. Addressing the Curse of Imbalanced Training Sets: One-Sided Selection, in: In Proceedings of the Fourteenth International Conference on Machine Learning. Morgan Kaufmann, pp. 179–186.

Laura, P., de Sousa, L., 2020. SoilGrids250m 2.0 - Clay content. https://doi.org/10.17027/ISRIC-SOILGRIDS.713396F7-1687-11EA-A7C0-A0481CA9E724

Li, W., Liu, C., Hong, Y., Saharia, M., Sun, W., Yao, D., Chen, W., 2016. Rainstorm-induced shallow landslides process and evaluation – a case study from three hot spots, China. Geomat. Nat. Hazards Risk 7, 1908–1918. https://doi.org/10.1080/19475705.2016.1179685

Liu, C., Li, W., Wu, H., Lu, P., Sang, K., Sun, W., Chen, W., Hong, Y., Li, R., 2013. Susceptibility evaluation and mapping of China's landslides based on multi-source data. Nat. Hazards 69, 1477–1495. https://doi.org/10.1007/s11069-013-0759-y

Lok Sabha (http://loksabhaph.nic.in/Questions/QResult15.aspx?qref=22874&lsno=17) [WWW Document], 2021. URL http://loksabhaph.nic.in/Questions/QResult15.aspx?qref=22874&lsno=17 (accessed 5.12.22).

Martha, T.R., Roy, P., Jain, N., Khanna, K., Mrinalni, K., Kumar, K.V., Rao, P.V.N., 2021. Geospatial landslide inventory of India—an insight into occurrence and exposure on a national scale. Landslides 18, 2125–2141. https://doi.org/10.1007/s10346-021-01645-1

Meena, S.R., Puliero, S., Bhuyan, K., Floris, M., Catani, F., 2022. Assessing the importance of conditioning factor selection in landslide susceptibility for the province of Belluno (region of Veneto, northeastern Italy). Nat. Hazards Earth Syst. Sci. 22, 1395–1417. https://doi.org/10.5194/nhess-22-1395-2022

Nadim, F., Kjekstad, O., Peduzzi, P., Herold, C., Jaedicke, C., 2006. Global landslide and avalanche hotspots. Landslides 3, 159–173. https://doi.org/10.1007/s10346-006-0036-1

Nguyen, H.M., Cooper, E.W., Kamei, K., 2011. Borderline over-sampling for imbalanced data classification. Int. J. Knowl. Eng. Soft Data Paradig. 3, 4. https://doi.org/10.1504/IJKESDP.2011.039875

Okalp, K., Akgün, H., 2016. National level landslide susceptibility assessment of Turkey utilizing public domain dataset. Environ. Earth Sci. 75, 847. https://doi.org/10.1007/s12665-016-5640-3

Peña, M.A., Brenning, A., 2015. Assessing fruit-tree crop classification from Landsat-8 time series for the Maipo Valley, Chile. Remote Sens. Environ. 171, 234–244. https://doi.org/10.1016/j.rse.2015.10.029

Pham, B.T., Pradhan, B., Tien Bui, D., Prakash, I., Dholakia, M.B., 2016a. A comparative study of different machine learning methods for landslide susceptibility assessment: A case study of Uttarakhand area (India). Environ. Model. Softw. 84, 240–250. https://doi.org/10.1016/j.envsoft.2016.07.005

Pham, B.T., Pradhan, B., Tien Bui, D., Prakash, I., Dholakia, M.B., 2016b. A comparative study of different machine learning methods for landslide susceptibility assessment: A case study of Uttarakhand area (India). Environ. Model. Softw. 84, 240–250. https://doi.org/10.1016/j.envsoft.2016.07.005

Pham, B.T., Tien Bui, D., Prakash, I., Dholakia, M.B., 2017. Hybrid integration of Multilayer Perceptron Neural Networks and machine learning ensembles for landslide susceptibility assessment at Himalayan area (India) using GIS. CATENA 149, 52–63. https://doi.org/10.1016/j.catena.2016.09.007

863 Piacentini, D., Troiani, F., Soldati, M., Notarnicola, C., Savelli, D., Schneiderbauer, S., Strada,
864   C., 2012. Statistical analysis for assessing shallow-landslide susceptibility in South
865   Tyrol (south-eastern Alps, Italy). Geomorphology 151–152, 196–206.
866   https://doi.org/10.1016/j.geomorph.2012.02.003
867 Poggio, L., de Sousa, L., 2020a. SoilGrids250m 2.0 - Sand content.
868   https://doi.org/10.17027/ISRIC-SOILGRIDS.713396FA-1687-11EA-A7C0-
869   A0481CA9E724
870 Poggio, L., de Sousa, L., 2020b. SoilGrids250m 2.0 - Silt content.
871   https://doi.org/10.17027/ISRIC-SOILGRIDS.713396FB-1687-11EA-A7C0-
872   A0481CA9E724
873 Pradhan, B., 2013. A comparative study on the predictive ability of the decision tree, support
874   vector machine and neuro-fuzzy models in landslide susceptibility mapping using GIS.
875   Comput. Geosci. 51, 350–365. https://doi.org/10.1016/j.cageo.2012.08.023
876 Raj, R., Saharia, M., Chakma, S., Rafieinasab, A., 2022. Mapping rainfall erosivity over India
877   using multiple precipitation datasets. CATENA 214, 106256.
878   https://doi.org/10.1016/j.catena.2022.106256
879 Ram, P., Gupta, V., 2022. Landslide hazard, vulnerability, and risk assessment (HVRA),
880   Mussoorie township, lesser himalaya, India. Environ. Dev. Sustain. 24, 473–501.
881   https://doi.org/10.1007/s10668-021-01449-2
882 Ramachandra, T.V., Aithal, Dr.B., Uttam, K., Joshi, niranjan. v, 2013. Prediction of Shallow
883   Landslide prone regions in Undulating Terrains. Disaster Adv. 6, 53–63.
884 Ramli, M.F., Yusof, N., Yusoff, M.K., Juahir, H., Shafri, H.Z.M., 2010. Lineament mapping
885   and its application in landslide hazard assessment: a review. Bull. Eng. Geol. Environ.
886   69, 215–233. https://doi.org/10.1007/s10064-009-0255-5
887 Reichenbach, P., Rossi, M., Malamud, B.D., Mihir, M., Guzzetti, F., 2018. A review of
888   statistically-based landslide susceptibility models. Earth-Sci. Rev. 180, 60–91.
889   https://doi.org/10.1016/j.earscirev.2018.03.001
890 Sahin, E.K., 2020. Assessing the predictive capability of ensemble tree methods for landslide
891   susceptibility mapping using XGBoost, gradient boosting machine, and random forest.
892   SN Appl. Sci. 2, 1308. https://doi.org/10.1007/s42452-020-3060-1
893 Sim, K.B., Lee, M.L., Wong, S.Y., 2022. A review of landslide acceptable risk and tolerable
894   risk. Geoenvironmental Disasters 9, 3. https://doi.org/10.1186/s40677-022-00205-6
895 Singh, A., Ranjan, R.K., Tewari, V.C., 2020. Spatio-temporal Variability of Landslides in
896   Sikkim Himalaya, India, in: Pal, I., von Meding, J., Shrestha, S., Ahmed, I., Gajendran,
897   T. (Eds.), An Interdisciplinary Approach for Disaster Resilience and Sustainability,
898   Disaster Risk Reduction. Springer, Singapore, pp. 219–234.
899   https://doi.org/10.1007/978-981-32-9527-8_13
900 Stanley, T., Kirschbaum, D.B., 2017. A heuristic approach to global landslide susceptibility
901   mapping. Nat. Hazards 87, 145–164. https://doi.org/10.1007/s11069-017-2757-y
902 Stein, C., 1956. Inadmissibility of the Usual Estimator for the Mean of a Multivariate Normal
903   Distribution. Proc. Third Berkeley Symp. Math. Stat. Probab. Vol. 1 Contrib. Theory
904   Stat. 3.1, 197–207.
905 Sterlacchini, S., Ballabio, C., Blahut, J., Masetti, M., Sorichetta, A., 2011. Spatial agreement
906   of predicted patterns in landslide susceptibility maps. Geomorphology 125, 51–61.
907   https://doi.org/10.1016/j.geomorph.2010.09.004
908 Thi Ngo, P.T., Panahi, M., Khosravi, K., Ghorbanzadeh, O., Kariminejad, N., Cerda, A., Lee,
909   S., 2021. Evaluation of deep learning algorithms for national scale landslide
910   susceptibility mapping of Iran. Geosci. Front. 12, 505–519.
911   https://doi.org/10.1016/j.gsf.2020.06.013
912 Valdiya, K.S., 2015. The Making of India: Geodynamic Evolution. Springer.

913   Wieczorek, G.F., 1996. LANDSLIDES: INVESTIGATION AND MITIGATION. CHAPTER
914   4 - LANDSLIDE TRIGGERING MECHANISMS. Transp. Res. Board Spec. Rep.
915   Yalcin, A., Reis, S., Aydinoglu, A.C., Yomralioglu, T., 2011. A GIS-based comparative study
916   of frequency ratio, analytical hierarchy process, bivariate statistics and logistics
917   regression methods for landslide susceptibility mapping in Trabzon, NE Turkey.
918   CATENA 85, 274–287. https://doi.org/10.1016/j.catena.2011.01.014
919   Yamazaki, D., Ikeshima, D., Tawatari, R., Yamaguchi, T., O'Loughlin, F., Neal, J.C.,
920   Sampson, C.C., Kanae, S., Bates, P.D., 2017. A high-accuracy map of global terrain
921   elevations. Geophys. Res. Lett. 44, 5844–5853.
922   https://doi.org/10.1002/2017GL072874
923   Youssef, A.M., Pourghasemi, H.R., 2021. Landslide susceptibility mapping using machine
924   learning algorithms and comparison of their performance at Abha Basin, Asir Region,
925   Saudi Arabia. Geosci. Front. 12, 639–655. https://doi.org/10.1016/j.gsf.2020.05.010
926